Acta Materialia 141 (2017) 183–192

Contents lists available at ScienceDirect

Acta Materialia

journal homepage: www.elsevier.com/locate/actamat

Full length article

Deformation of small-volume Al-4Cu alloy under electron beam irradiation

Shi-Hao Li, Wei-Zhong Han*, Zhi-Wei Shan

Center for Advancing Materials Performance from the Nanoscale (CAMP-Nano) & Hysitron Applied Research Center in China (HARCC), State Key Laboratory for Mechanical Behavior of Materials, Xi'an Jiaotong University, Xi'an 710049, China

ARTICLE INFO

Article history:
Received 28 June 2017
Received in revised form
9 September 2017
Accepted 10 September 2017
Available online 12 September 2017

Keywords:
Electron beam irradiation
Al oxide shell
Strain rate sensitivity
Activation volume
Ductility

ABSTRACT

Energetic electron beams (e-beams) are used in the welding, 3D printing and imaging of various materials. It is commonly accepted that the e-beam irradiation inside transmission electron microscope has a negligible effect on the intrinsic mechanical properties of small-volume metallic materials during *in situ* investigation. However, as small-volume Al is usually covered by a thin layer of native oxide, we show here that high-energy (200 keV) e-beam irradiation can dramatically alter the deformation behavior. E-beam irradiation can drastically rejuvenate the amorphous structure of the oxide layer, producing a defective interface/surface, and promoting the transition of the deformation mode from internal dislocation multiplication to interface-dominated dislocation nucleation mediated plasticity, as indicated by the enhanced strain rate sensitivity and reduced activation volume. Moreover, the amorphous oxide layer undergoes viscous flow under the e-beam irradiation, such that nanoscale single-crystal Al confined by a 29% volume fraction of native oxide shell exhibits more than 60% uniform elongation.

1. Introduction

Small-volume materials with micro- or nano-sized sample dimensions usually exhibit unique mechanical properties that are distinct from those of their bulk counterparts [1,2]. However, low deformation stability (frequent strain bursts), near zero strain hardening and limited uniform elongation plague their applications [1–9]. *In situ* mechanical tests under electron beam (e-beam) imaging have been performed to study the microstructural evolution and mechanical properties of various kinds of small-volume materials [1–9]. Dynamic videos acquired during *in situ* investigations shed light on the deformation mechanisms of nanoscale materials, guiding the researchers and engineers to design and fabricate mechanically robust micro-and nano-scale devices.

The e-beam imaging frequently used for *in situ* studies causes irradiation damage to the nanoscale samples due to the collision produced by high energy electrons [10–13]. In general, e-beam irradiation has a more significant effect on small-volume amorphous oxides than on metals due to their distinct average displacement threshold energies and to the nature of atomic bonding. Several investigations have indicated that e-beam irradiation could exert a non-negligible influence on the intrinsic mechanical properties of nanoscale oxides [14–17]. Under low-intensity e-beam irradiation, normally brittle nanoscale amorphous silica exhibited large homogeneous plastic strains or superplastic deformation at room temperature (RT) [15]. Atomistic simulations revealed that high-energy e-beam-induced radiation defects assisted the atoms in overcoming the energy barrier for bond switching [15,16,18,19] during mechanical loading, which is beneficial for healing plastic damage and increasing the plastic flow, thus producing very high homogeneous plasticity [15]. As such, e-beam irradiation has a significant effect on the deformation of silica and related materials, and is useful for processing conventionally brittle amorphous oxides.

However, much less investigation has been carried out on the effect of e-beam irradiation on the deformation of small-volume metals. Based on the empirical assumption that the high-energy e-beam does not alter the intrinsic mechanical properties of small-volume metals, the effects of e-beam irradiation are usually ignored. Recently, Sarkar et al. [20] reported that e-beam exposure could induce marked stress relaxation and anomalous sample necking in Al films. It is claimed that e-beam exposure could assist in dislocation activation and promote the depinning of dislocations

* Corresponding author.
E-mail address: wzhanxjtu@mail.xjtu.edu.cn (W.-Z. Han).

http://dx.doi.org/10.1016/j.actamat.2017.09.015
1359-6454/

trapped at defects, thereby giving rise to the stress relaxation and abnormal necking. This explanation is similar to the mechanism of electric current pulse assisted dislocation activation [21], which is drastically different from the mechanism of e-beam-induced knock-on damage.

Nevertheless, in general, Al is always covered by a very thin layer of native oxide [22–28]. Recently, it was found that nanoscale Al-4Cu alloys show unprecedented strength and toughness due to the strong confinement imposed by the ultrathin layer of native Al oxide shell [22]. Since the oxide layer is sensitive to e-beam irradiation, the intrinsically brittle oxide layer may deform through bond switching under e-beam irradiation, via the same mechanism unveiled in silica [15], which could be the origin of the e-beam-induced softening in the plastic deformation of nanoscale Al thin film [20]. In addition, recent atomic simulations revealed that the native Al oxide shell could also enhance the ductility of Al nanowires via *in situ* oxidation when undergoing tensile deformation at a low strain rate [23,24]. Therefore, the bond switching or oxygen diffusion induced self-healing could significantly improve the deformability of nanoscale Al. However, these processes occur readily only under specific conditions, such as under e-beam exposure/in an oxygen atmosphere and at low loading rate [18,19,23,24]. As a result, the deformation behavior of small-volume metal-oxide shell "composites" [22–29] is likely strain rate dependent. However, so far no research has been performed in this direction.

In this work, we performed systematic *in situ* tensile testing on a group of small-volume Al-4Cu specimens under e-beam-on/off conditions and at different strain rates to uncover the combined effects of e-beam and strain rate on the plastic deformation of small-volume Al alloy covered by the naturally formed oxide shell. We found that e-beam irradiation could drastically enhance the deformability of small-volume Al alloy below a critical strain rate.

2. Experimental design

In this study, we chose peak-aged Al-4Cu alloy as our model material. Small-volume Al-4Cu alloys with native oxide shells exhibit stable and homogeneous deformation with no apparent strain burst, which makes them suitable to evaluate the effect of high-energy e-beam irradiation [22]. A series of single-crystal Al-4Cu tensile samples (Fig. 1a and b) were fabricated by using focused ion beam (FIB) micromachining for *in situ* tensile tests. The ion beam current was reduced to 9.7 pA for the final thinning to minimize possible FIB-induced surface damage. Dense plate-shaped shear-resistant precipitates θ' (Al_2Cu) distributed on the $\{001\}_\alpha$planes of Al matrix can be observed in the Al-4Cu sample (Fig. 1b). More details about these shear-resistant precipitates can be found elsewhere [30,31]. The dimensions of the tensile samples were measured before tensile tests under a scanning electron microscope (SEM) to quantify the stress-strain response. For this study, a fixed tensile sample size of 2 μm gauge length, 0.4 μm width and 0.2 μm thickness was used (Fig. 1). Thus, all the samples have an equivalent sample size D ($D\equiv\sqrt{A}$, where A is the cross-section area of tensile samples) of 283 nm.

In situ tensile tests were carried out using a Hysitron PicoIndentor (PI95) equipped with a tungsten grip inside an FEG JEOL 2100F transmission electron microscope (TEM, 200 kV) under displacement control. Real-time data on the displacement and force were recorded during tensile loading. We compared the tensile test responses under beam-on and beam-off conditions. For beam-on tests, all tensile samples were exposed to the imaging e-beam during mechanical testing. In contrast, the e-beam was blocked by the condenser lens aperture during the tensile tests for the beam-off condition. The displacement of the grip, which is approximately equal to the magnitude of displacement in the sample gauge section, was used to calculate the strain of the tensile samples. The yield point was defined as the point where the derivative of the stress-stain curve deviates from the elastic deformation, and the corresponding stress is yield strength. Tensile tests with different strain rates were performed to explore the strain rate effects; the displacement rate was varied from 1 nm s^{-1} to 100 nm s^{-1}, corresponding to strain rates of $5\times10^{-4}\sim5\times10^{-2}s^{-1}$. For each testing condition, at least three samples were used to obtain a reliable stress-strain response.

To further investigate the effect of high-energy e-beam irradiation, we fabricated some single-crystal Al samples in a push-to-pull (PTP) sample geometry [32] and performed tensile tests under both beam-off and beam-on conditions. The size of the cross-section of the PTP samples was approximately 55 nm × 55 nm. Since the thickness of the native oxide shell was constant (about 4.3 nm), the volume fraction of oxide shell in the PTP samples was ~29% [22], which was much larger than that in normal micro-scale tensile samples (~6%). The displacement rate was set to be 1 nm s^{-1} in the PTP tests, corresponding to a strain rate of ~1×10^{-3} s^{-1}.

3. Experimental results

3.1. The tensile behavior of small-volume Al alloy under beam-on/off conditions

Fig. 1a and b display the typical SEM and TEM images of a single-crystal Al-4Cu tensile sample. Plate-shaped shear-resistant precipitates θ' can be observed in the sample. In addition, we note that a layer of ultrathin and fully dense amorphous native oxide shell covers the tensile sample (Fig. 1c). The surface of Al will instantly form a layer of native oxide shell once exposed to oxygen, even in an environment with the partial pressure of oxygen as low as 10^{-8} Torr [22–28]. Regardless of the sample morphology and size, the native oxide shell with a homogeneous thickness of ~4.3 nm always covers the whole tensile sample.

We first performed *in situ* tensile tests under the beam-off condition at four different strain rates, ranging from $\sim5\times10^{-4}$ s^{-1} to $\sim5\times10^{-2}s^{-1}$. Fig. 2a shows four typical true stress-strain curves of the small-volume Al-4Cu alloy tensile samples at different strain rates. All tensile samples delivered stable and continuous plastic deformation without marked strain bursts or load drops, which was consistent with early studies [22]. In addition, it seems that the Young's modulus shows a weak dependence on the strain rates for beam off tests, as displayed in Fig. 2a. However, based on the character of nanomechanical test, the small variation of the Young's modulus is not related to the strain rate, but likely induced by the environment noise, which is common in *in situ* test. In general, the four tensile stress-strain curves show similar features, such as very similar yield strength (0.42 GPa-0.52 GPa), flow stress and ultimate tensile strength (UTS) (0.66 GPa-0.74 GPa).

For comparison, tensile tests were carried out subsequently under the beam-on condition at the four different strain rates. Four typical true stress-strain curves of the tensile tests under the beam-on condition are displayed in Fig. 2b. It is obvious that the stress-strain curves vary significantly for various strain rates under beam-on conditions. Under e-beam irradiation, the flow stress of small-volume Al-4Cu decreases markedly as the strain rate decreases, while the fracture strain increases significantly with decreasing strain rate. The UTS of the sample tested at $5\times10^{-3}s^{-1}$ is approximately 0.75 GPa, which is much higher than the UTS (~0.48 GPa) of the sample tested at 5×10^{-4} s^{-1}. The fracture strain of the sample measured at 5×10^{-4} s^{-1} is ~17%, which is more than two times higher than that of samples loaded at 5×10^{-3} s^{-1}.

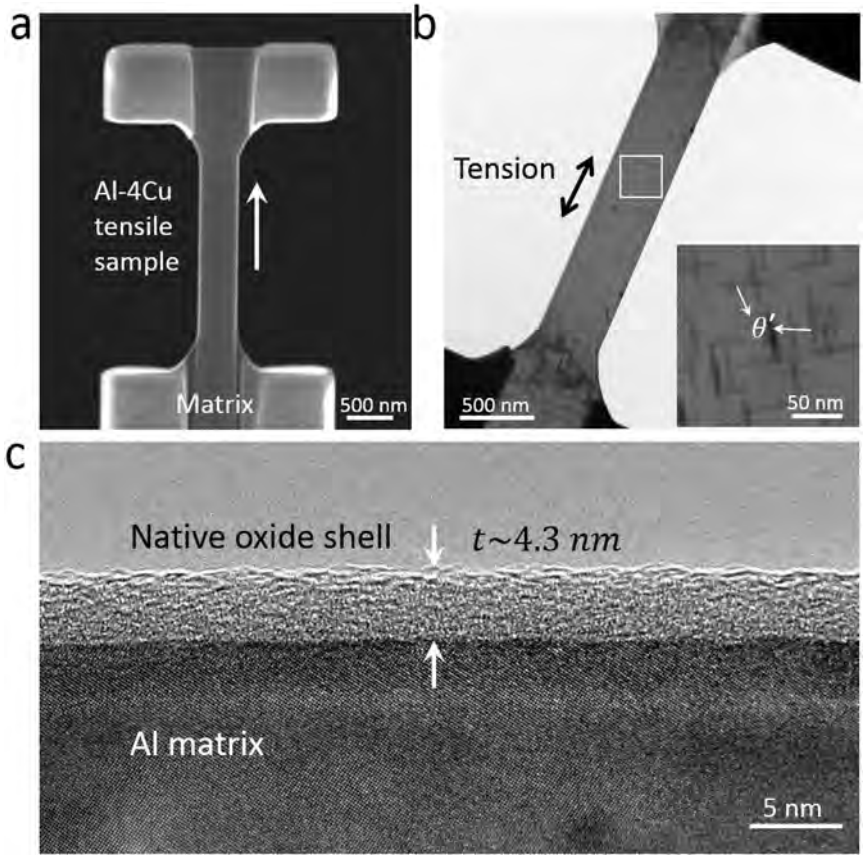

Fig. 1. Morphology and microstructure of nanoscale Al-4Cu single crystal tensile sample. **(a)** SEM image of nanoscale Al-4Cu sample; **(b)** TEM image of nanoscale Al-4Cu sample. The insert is the enlarged TEM image showing the shear-resistant precipitates (θ'); **(c)** Amorphous native oxide shell with constant thickness of 4.3 nm formed on the surface of nanoscale Al-4Cu sample.

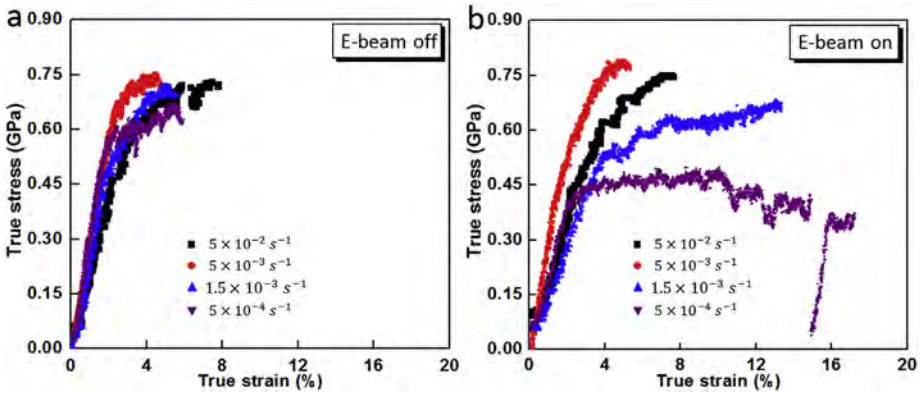

Fig. 2. Typical true stress-strain curves of nanoscale Al-4Cu samples measured at different strain rates under beam on/off conditions. **(a)** True stress-strain curves of nanoscale Al-4Cu tested under beam-off condition. **(b)** True stress-strain curves of nanoscale Al-4Cu tested under beam-on condition.

Interestingly, the tensile deformation behaviors of small-volume Al-4Cu samples deformed at higher strain rates (5×10^{-2} and 5×10^{-3} s^{-1}) under the beam-on condition are similar to those of samples tested under the beam-off condition (Fig. 2a). However, for lower strain rates (1.5×10^{-3} and 5×10^{-4} s^{-1}), samples tested under the beam-on condition exhibit much lower strength but better plastic deformation ability. This behavior of small-volume Al-4Cu is quite similar to the plastic deformation of nanoscale amorphous silica and Al film under e-beam exposure [15,16]. Based on the comparison above, high-energy e-beam irradiation can dramatically change the mechanical behavior of small-volume Al-4Cu alloy, especially at lower strain rates.

To further study the effect of high-energy e-beam irradiation on small-volume Al-4Cu at different strain rates, true stress-strain curves of tensile tests at different strain rates (5×10^{-3} s^{-1} and 5×10^{-4} s^{-1}) under both beam-off and beam-on conditions are compared, as shown in Fig. 3. The samples tested at 5×10^{-3} s^{-1} exhibit similar true stress-strain curves under both e-beam-on and e-beam-off conditions, indicating that the e-beam has less effect on the deformation of small-volume Al-4Cu at higher strain rates. Both

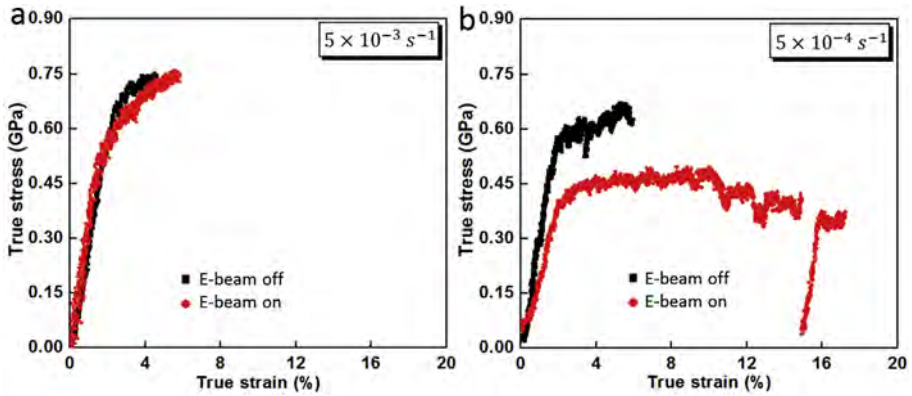

Fig. 3. Comparison of the true stress-strain curves of nanoscale Al-4Cu under beam on/off conditions with the same strain rate. **(a)** True stress-strain curves of nanoscale Al-4Cu tested at 5×10^{-3} s^{-1}. **(b)** True stress-strain curves of nanoscale Al-4Cu tested at 5×10^{-4} s^{-1}.

of the tensile samples yield at approximately 0.5 GPa, followed by a stable and continuous strain hardening period, and fracture at a UTS of ~0.75 GPa. However, the tensile samples strained at 5×10^{-4} s^{-1} show completely different deformation behaviors under e-beam-on/off conditions. Under slow strain rate and beam-off condition, these samples show significant strain hardening after yielding, then fracture at a UTS of 0.66 GPa with a total elongation of ~6.5%. In contrast, under beam-on and low strain rate conditions, the samples exhibit lower yield strength, as shown in Fig. 3b (red curve). It should be mentioned that there is a small variation of the measured Young's modulus for the samples tested at low strain rate under e-beam irradiation (Figs. 2b and 3b), which can be attributed to the velocity-limited viscous flow of amorphous oxide shell due to e-beam irradiation. In general, a slight change of the Young's modulus of the surface amorphous oxide shell will alters the Young's modulus of the small-volume Al sample [22]. After yielding, a long strain hardening stage with a low strain hardening rate dominates the plastic flow. The samples then fracture with an UTS of 0.48 GPa and a total strain of 17%.

Fig. 4a and Movie S1 display the deformation behavior of samples strained at 5×10^{-3} s^{-1} under the beam-on condition. The small-volume Al-4Cu single-crystal with [$\bar{6}$65] orientation yields at a strain of ~2.1% (Fig. 4a-II). As the tensile test proceeds further, the tensile sample shows uniform deformation (Fig. 4a-III). Upon further elevating the strain to 5.6%, the sample displays brittle fracture with no necking stage (as marked by the black arrows in Fig. 4a-IV), and the final fracture plane is almost perpendicular to the loading axis (Fig. 4a-IV and Movie S1). This behavior is similar to that observed in our early studies [22]. In contrast, a nanoscale Al-4Cu tensile sample with the same orientation strained at 5×10^{-4} s^{-1} under the beam-on condition shows different deformation behavior, as demonstrated in Fig. 4b and Movie S2. The small-volume Al-4Cu yields at a strain of 2.7%, following a long uniform deformation stage with a high strain of up to 15.2%. In contrast to the catastrophic brittle fracture tested with a strain rate of 5×10^{-3} s^{-1}, the sample shows an obvious necking deformation stage before the final fracture, as illustrated in Fig. 4b-IV. The total elongation is approximately 30%, which is much higher than that of

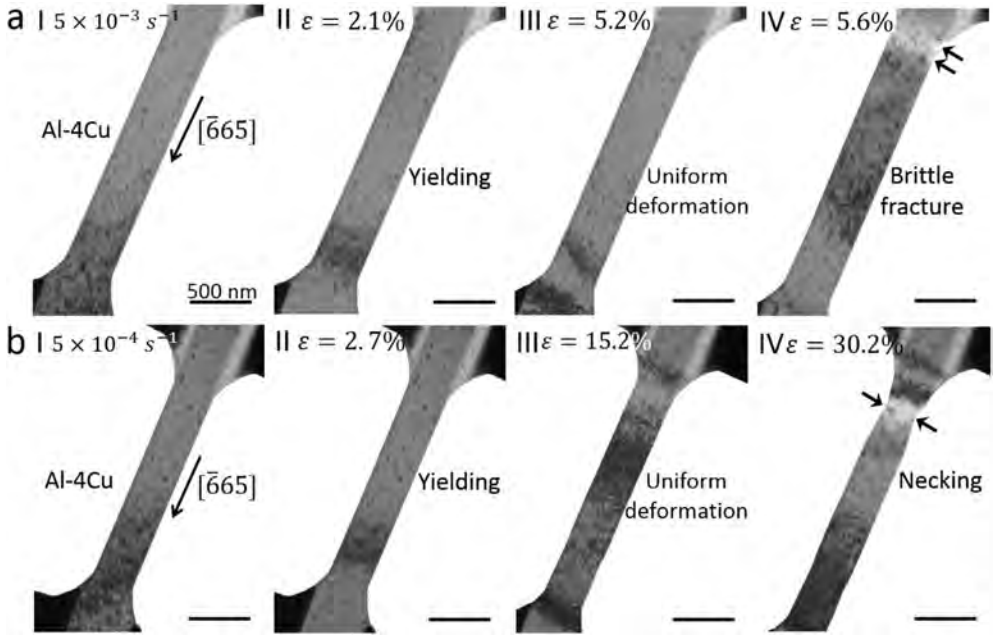

Fig. 4. Deformation processes of nanoscale Al-4Cu at different strain rates under beam-on condition. **(a)** Deformation and failure of nanoscale Al-4Cu tested at 5×10^{-3} s^{-1}. **(b)** Deformation and failure of nanoscale Al-4Cu tested at 5×10^{-4} s^{-1}.

the former sample. The fracture of the native oxide shell leads to the brittle fracture of small-volume Al-4Cu [22]. Thus, it is interesting to find that tensile samples with $D = 283$ nm show ductile failure when tested at 5×10^{-4} s^{-1} under the beam-on condition. In contrast to the brittle fracture of samples under the beam-off condition regardless of strain rate, these results indicate that e-beam irradiation could promote the plastic deformation of small-volume Al-4Cu, especially at a slow loading rate.

Supplementary data related to this article can be found online at http://dx.doi.org/10.1016/j.actamat.2017.09.015.

To quantitatively investigate the effect of high-energy e-beam irradiation on the mechanical properties of small-volume Al-4Cu, the yield strength, UTS and fracture strain of tensile samples measured under various strain rates and e-beam conditions are summarized in Fig. 5. In general, under the beam-on condition, small-volume Al-4Cu exhibits lower yield strength and UTS but higher fracture strain than under the beam-off condition. This trend is obvious at low strain rates and gradually disappears with increasing strain rate, indicating the marked influence of e-beam condition and strain rate on the mechanical properties of small-volume Al-4Cu samples. In addition, a trend of higher strength with higher strain rate can be identified in the tests under both beam-on and beam-off conditions, which is consistent with other investigations on Al [33–36]. However, it should be noted that the yield strength and UTS of samples tested under the beam-on condition increase more rapidly with increasing strain rate than the beam-off condition, which demonstrates that high-energy e-beam irradiation enhances the strain rate sensitivity of small-volume Al-4Cu alloy.

3.2. The strain rate sensitivity of small-volume Al-4Cu alloy

The effects of grain size [33–39], sample size [40,41], microstructures [42–46], and temperature [47] on the strain rate sensitivity of metals have been extensively explored, however, the effect of e-beam irradiation on the strain rate sensitivity of small-volume metals has not been investigated yet. Notably, small-volume Al-4Cu samples strained at $5 \times 10^{-4} s^{-1}$ under e-beam irradiation deliver dramatically higher fracture strain, which is likely related to the viscous flow of native oxide shell [23]. We subsequently choose the yield strength, the flow stress at 3% strain (σ_3) and the flow stress at 5% strain (σ_5) as references to quantify the strain rate sensitivity of small-volume Al-4Cu alloy. The variation of stress with strain rate is summarized in the log-log plots, as shown in Fig. 6 for both e-beam-off and e-beam-on conditions. The strain rate sensitivity exponents $m=\frac{\partial \ln \sigma}{\partial \ln \dot{\varepsilon}}$ for both e-beam-off and e-beam-on conditions are measured by linear fitting. It seems that two distinct strain rate sensitivity values can be determined regardless of the stress selected and the e-beam conditions. For strain rate-$\dot{\varepsilon} \leq 5 \times 10^{-3}$ s^{-1}, a higher strain rate sensitivity can be identified for both beam-off and beam-on conditions. For strain rate $\dot{\varepsilon} \geq 5 \times 10^{-3}$ s^{-1}, near-zero or negative strain rate sensitivity can be determined. In the following, we mainly focus on the strain rate sensitivity of samples deformed at strain rates ranging from 5×10^{-4} to 5×10^{-3} s^{-1}. Compared to the beam-off condition, samples tested under the beam-on condition display much higher strain rate sensitivity. When σ_3 is chosen as the reference, the strain rate sensitivity exponent m for the beam-on condition is 0.147, which is three times the value of $m = 0.044$ for the beam-off condition. The strain rate sensitivity exponents calculated by choosing yield strength or σ_5 as the reference display a similar trend (Fig. 6a and b). Based on the comparison above, it is evident that e-beam irradiation dramatically enhances the strain rate sensitivity of small-volume Al-4Cu alloy.

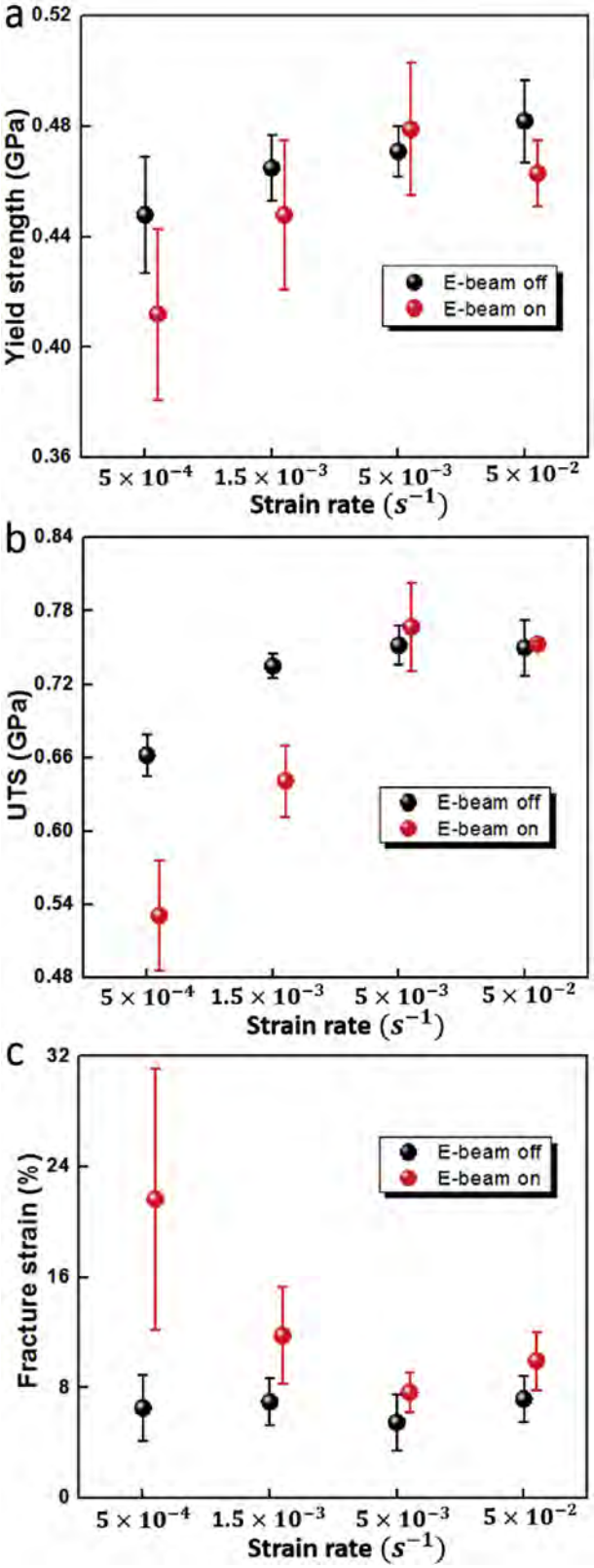

Fig. 5. The variation of yield strength **(a)**, UTS **(b)** and fracture strain **(c)** of nanoscale Al-4Cu with the testing strain rates and e-beam conditions.

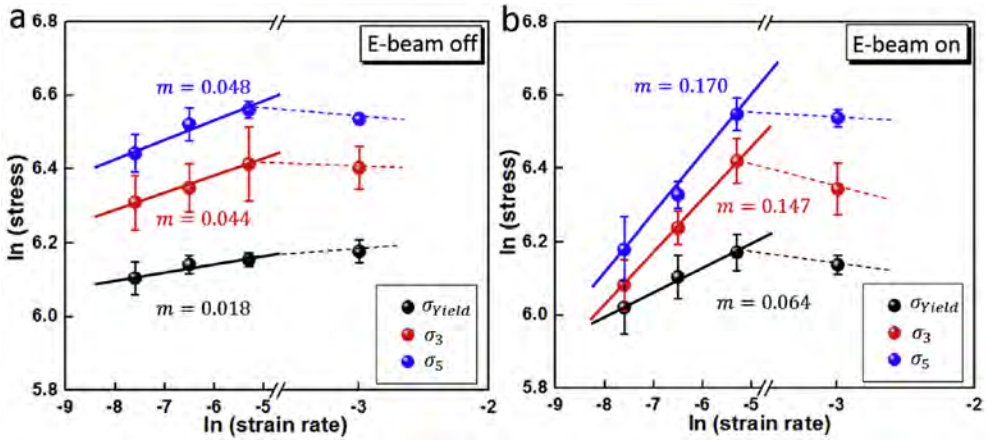

Fig. 6. Strain rate sensitivity of nanoscale Al-4Cu loaded under beam-off **(a)** and beam-on **(b)** conditions. Yield strength (σ_{Yield}), flow stress at 3% strain (σ_3) and flow stress at 5% strain (σ_5) are selected as references to calculate the strain rate sensitivity exponent m. Two stages of strain rate sensitivity can be divided at $\dot{\varepsilon} = 5 \times 10^{-3}$ s^{-1} ($ln\,\dot{\varepsilon} = -5.3$) according to log-log plots. For strain rate $\dot{\varepsilon} \leq 5 \times 10^{-3}$ s^{-1}, nanoscale Al-4Cu samples show much higher strain rate sensitivity under beam-on condition. For strain rate $\dot{\varepsilon} \geq 5 \times 10^{-3} s^{-1}$, near zero or negative strain rate sensitivity can be measured.

3.3. *Tensile tests on ultrathin Al with large volume fraction of native oxide shell*

Fig. 7a and Movie S3 show the deformation behavior of small-volume Al with a large fraction (29%) of native oxide shell under e-beam irradiation. Before straining, the width of PTP sample is ~55 nm (Fig. 7a-I). Upon the gradual increase of the strain to 15.8%, the PTP sample displays uniform deformation, and the width decreases to 52 nm (Fig. 7a-II). Upon further elevation of the strain to 60.2%, the PTP sample still displays continuous uniform deformation with the final sample width of 47 nm (Fig. 7a-III). When the strain reaches 82.6%, a liquid-like deformation behavior is demonstrated in the fracture front of nanoscale Al (Fig. 7a-IV), which is quite similar to the deformation behaviors of sub-10-nm crystalline silver particles [48] and amorphous $Al_{90}Fe_5Ce_5$ [49]. For comparison, we also conducted PTP tests under the beam-off condition with a similar strain rate. The e-beam is blocked off by the condenser lens aperture. To observe the deformation behavior of nanoscale Al, we removed the condenser lens aperture every 15 s and took a TEM image of the tensile sample, and then the e-beam was immediately blocked off after imaging. Fig. 7c shows typical TEM images acquired during the test. With a gradual increase of the strain to 9.6%, a large shear offset can be seen clearly in the middle part of the sample (Fig. 7c-II), indicating earlier localized

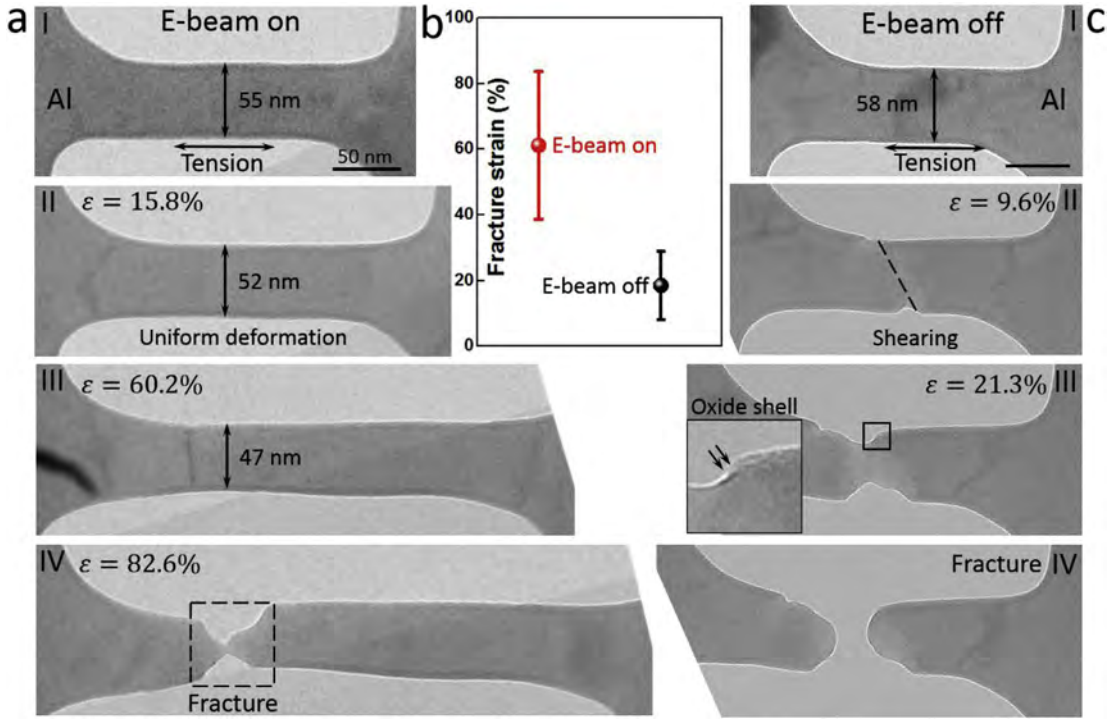

Fig. 7. Push-to-pull (PTP) tests on ultrathin Al single crystal covered by large volume fraction of amorphous native oxide shell. **(a)** PTP samples show high fracture strain after a large uniform elongation under beam-on condition. **(b)** Fracture strain of samples tested under beam-on condition is much higher than that of samples loaded under beam-off condition. **(c)** PTP samples show brittle fracture after a short uniform elongation under beam-off condition.

deformation of the PTP sample under the beam-off condition. Upon further elevation of the strain to 21.3%, the broken oxide shell can be observed on the fracture front of the sample (Fig. 7c-III), indicating brittle fracture of the oxide shell. Then, the PTP sample fractures completely as the strain increases further (Fig. 7c-IV). Fig. 7b lists the fracture strains of PTP samples tested under beam-off (black point) and beam-on (red point) conditions. It is obvious that the samples tested under e-beam irradiation display much larger fracture strain.

Supplementary data related to this article can be found online at http://dx.doi.org/10.1016/j.actamat.2017.09.015.

4. Discussion

Compared to the nanoscale Al-4Cu alloy deformed under the beam-off condition, the samples tested under the beam-on condition exhibit improved deformability, especially at low strain rates. The variation in the mechanical properties of small-volume Al-4Cu alloy can be attributed to the high-energy e-beam irradiation. In the following, we will rationalize the effect of e-beam irradiation and strain rate on the mechanical behavior of small-volume Al alloy.

4.1. Negligible temperature increase under low-intensity e-beam irradiation

The effect of e-beam irradiation on the temperature evolution in small-volume Al alloy will be discussed. High-intensity e-beams have been employed to conduct nanoscale welding, create atomic-scale structures and print nanoscale patterns [50]. The incident electrons excite the medium as they travel through the sample and transmit part of energy to the matrix, which will enhance the temperature of the sample if the e-beam intensity is high. In our tests, the samples strained at 5×10^{-4} s^{-1} under the beam-on condition show enhanced deformability with an average fracture strain of ~20%, which is approximately three times higher than that of the samples tested without e-beam exposure (Figs. 5c and 7). One of frequently asked question is whether the high deformability is caused by the e-beam irradiation induced temperature change?

The e-beam-induced temperature increase in small-volume Al-4Cu alloy can be estimated. The incident electrons transmit part of their energy to the sample and likely induce heating during imaging. The energy loss of an electron per unit length can be defined as [15],

$$Q = Q_c + Q_r \tag{1}$$

where Q_c is the collision stopping power and Q_r is the radiative stopping power. As copper atoms in Al-4Cu alloy have negligible influence on Q_c and Q_r, we simply adopt the Q_c and Q_r of pure Al for the current estimation. The collision stopping power is ~2.17 MeV cm^2 g^{-1} and the radiative stopping power is ~8.34×10^{-3} MeV cm^2 g^{-1} for pure Al [51]. Hence the energy transition density rate can be written as [15],

$$H = \frac{QJ}{e} \tag{2}$$

where J is the e-beam current density, and e is the elementary charge (1.6×10^{-19} C). We adopt a fixed e-beam current intensity of 0.048 A cm^{-2} during our beam-on test. Thus, the energy transition density rate is about 2.81×10^{11} W m^{-3}. The H calculated above is the energy transfer rate from high-energy incident electrons to nanoscale samples. Since all the nanoscale Al-4Cu tensile samples were fabricated by FIB micromachining on a piece of Al-4Cu substrate with a size of 3 mm×2 mm×50 μm, the volume of the substrate is approximately nine orders of magnitude larger than the volume of the nanoscale samples. Because of the relatively large volume of Al-4Cu substrate and the low e-beam current intensity used, the temperature of the Al-4Cu substrate would maintain almost constant (at RT) during the tensile tests. Thus, the e-beam irradiation-induced heating in nanoscale samples during the testing will transfer to the substrate instantly. When this heating-dissipation process reaches equilibrium, the temperature increase in the tensile samples can be estimated as [15],

$$\Delta T = \frac{HV}{GA} \tag{3}$$

where V is the volume of the sample under e-beam irradiation, G is the contact thermal conductance, and A is the area of thermal conductance. In this work, we define V approximately as the volume of the gauge section and A as the cross-section area of the gauge section of the tensile sample. It should be noted that the contact thermal conductance G is highly dependent on the state of the interface [52,53]. For instance, the contact thermal conductance G is approximately 10–1000 MW m^{-2} K^{-1} for ideal contact interfaces, while G is smaller than 0.01 MW m^{-2} K^{-1} for rough interfaces [52,53]. Since all nanoscale Al-4Cu is fabricated directly on the Al-4Cu substrate, the contact interfaces can be considered to be extremely smooth. Therefore, the contact thermal conductance G in our work should be in the range of 10–1000 MW m^{-2} K^{-1}. If we take the lower bound of this range, which means that $G = 10$ MW m^{-2} K^{-1}, thenΔT is ~0.056 K. Hence there is a negligible temperature increase during the tensile tests. If we take the upper bound of the contact thermal conductance, the calculated ΔT is two orders of magnitude smaller. Based on the analysis above, we conclude that the low e-beam current intensity used in our work cannot induce significant heating in the small-volume Al-4Cu alloy. The temperature of the small-volume samples remains constant near RT during all the tests.

4.2. Dislocation nucleation mechanism transition induced by e-beam irradiation

Dislocation nucleation plays a critical role in the deformation of both bulk and small-volume samples. In general, the dislocation nucleation process is mainly controlled by two factors, the athermal strength and the thermal activation [47,54]. For a given temperature T and strain rate $\dot{\varepsilon}$ during plastic deformation, the athermal stress σ needed for dislocation nucleation can be written as [54],

$$\sigma = \frac{Q^*}{\Omega} - \frac{k_B T}{\Omega} ln \frac{k_B T N \upsilon_0}{E \dot{\varepsilon} \Omega} \tag{4}$$

where Q^* is the activation energy for dislocation nucleation without any applied stress. Ω is the activation volume, Q^*/Ω is the stress required for dislocation nucleation at 0 K, k_B is the Boltzmann constant, N is the number of dislocation nucleation sites, υ_0 is the attempt frequency for dislocation nucleation, and E is the Young's modulus. According to the last term on the right side of equation (4), which represents the thermal fluctuation contribution to dislocation nucleation, the stress required for dislocation nucleation shows high dependence on the temperature T, the activation volume Ω and the strain rate $\dot{\varepsilon}$. Both experiments [47] and simulations [54] have shown that deformation temperature has a significant influence on the flow stress of samples. However, all tensile tests in this work were performed at RT. In addition, the e-beam irradiation induces only a negligible temperature increase (less than 1 K) in the small-volume samples. Therefore, the significant variation of the flow stress in the nanoscale Al-4Cu samples in the

current investigation has little to do with temperature.

In general, the magnitude of the activation volume is often a direct reflection of the dislocation nucleation mechanisms in bulk and small-volume metals [41,54], for example, the Frank-Read (F-R) source has an activation volume of hundreds or even thousands of b^3, where b is the Burgers vector. However, for small-volume samples, there are two types of dislocation nucleation mechanisms. One is dislocation nucleation through spiral sources or single-arm sources (SAS, which can be considered truncated F-R sources) [54]. This phenomenon has been observed in samples of sub-micrometer size [28,55]. The other is dislocation nucleation from the surface/interface [23,41], which usually occurs in samples with sizes of tens of nanometers [56,57]. The activation volume for the former mechanism ranges from tens of b^3 to hundreds of b^3, while the latter generally corresponds to activation volumes of less than $10b^3$[41,54]. A transition from the former mechanism to the latter mechanism may occur with further reduction the sample size [41].

According to equation (4), the strain rate $\dot{\varepsilon}$ inside the logarithm term may have a limited influence on the stress required for dislocation nucleation when the activation volume is quite large, resulting in low strain rate sensitivity. However, the flow stress will have a high dependence on the strain rate when the activation volume is extremely small, resulting in higher strain rate sensitivity. If there is a transition from SAS-dominated dislocation nucleation to surface/interface-mediated dislocation nucleation, it will manifest in an obvious increase in the strain rate sensitivity [41,54]. For current tests, the activation volumes of small-volume Al-4Cu alloy samples tensile under e-beam-on and e-beam-off conditions are estimated according to the equation below [42,58]:

$$\Omega = \frac{\sqrt{3}k_B T}{\sigma}\frac{\partial \ln(\dot{\varepsilon})}{\partial \ln(\sigma)} \tag{5}$$

The flow stress at 3% strain (σ_3) was used to quantify the activation volume. Fig. 8 shows the distinct activation volume for dislocation nucleation under e-beam on/off conditions. The activation volumes of the samples tested under the beam-off condition are $\sim 12b^3$, indicating that the operation of SAS likely controls the plasticity of the nanoscale Al-4Cu alloy. Notably, the samples deformed under the beam-on condition show much smaller activation volumes, only ~$4b^3$, indicating that interface/surface-mediated dislocation nucleation dominated the plasticity [41,54].

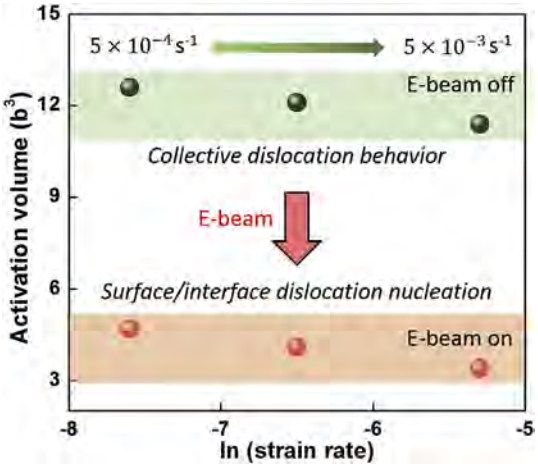

Fig. 8. The activation volume of dislocation nucleation in nanoscale Al-4Cu under beam on/off conditions in the strain rate ranging from 5×10^{-4} to 5×10^{-3} s^{-1}. The activation volume was estimated based on flow stress at 3% strain.

Since the volume fraction of the oxide shell in these samples is only 6.3%, the contribution of the oxide shell to the reduction of the average activation volume is limited, while the transition of the dislocation nucleation model is the main factor. Based on the analysis above, the high-energy e-beam could tune the dislocation nucleation mechanism and lead to much higher strain rate sensitivity in small-volume Al-4Cu alloy (Fig. 6).

For illustration, we plot cartoons of the two different dislocation nucleation mechanisms, as shown in Fig. 9. Under the beam-off condition, SAS is the dominant dislocation nucleation model (Fig. 9a). During plastic straining, the dislocation (green curves) pinned by one pinning point (gray dots) has two equilibrium positions (stable and unstable) [41], which are labeled in Fig. 9a. Under a given stress, some thermal fluctuations are required to move the dislocation from the stable equilibrium position to the unstable equilibrium position to generate new dislocations. The area swept by the dislocation during dislocation propagation between the stable and unstable equilibrium positions is defined as the activation volume (light orange area in Fig. 9a), which is on the order of $12b^3$. Fig. 9b illustrates the interface mediated dislocation nucleation under e-beam irradiation. With e-beam irradiation, numerous disordered local regions along the interface were produced, which are most likely dislocation nucleation sites [23]. Hence, the interface of the Al-4Cu matrix and the native oxide shell provides profuse dislocation nucleation sites with higher thermal activation, and thus, the stress required for dislocation nucleation under the beam-on condition is much lower than that under the beam-off condition, resulting in a lower yield strength (Fig. 5a). For the above reasons, a transition of dislocation nucleation from SAS to interface-dominated dislocation nucleation could occur in small-volume Al-4Cu (Fig. 9). These analyses indicate that high-energy e-beam irradiation can promote transition of the deformation model from internal dislocation multiplication to interface-dominated dislocation nucleation-mediated plasticity.

4.3. Viscous flow of amorphous oxide shell induced by e-beam irradiation

In this study, the samples tested below 5×10^{-3} s^{-1} under the beam-on condition show enhanced deformability compared with samples tested under the beam-off condition. Viscous flow of the native amorphous oxide shell under the e-beam-on condition is the main reason for the high ductility demonstrated by the nanoscale Al and Al-4Cu alloy. Many small-volume amorphous oxides, such as silica, show low strength but quite high ductility under e-beam irradiation at temperatures far below their glass transition points [15]. The mechanism underlying this phenomenon is the viscous flow of amorphous materials under e-beam irradiation. In this work, the high-energy (200 keV) incident e-beam could promote the cleavage of Al-O covalent bonds, forming abundant dangling Al and O bond pairs in the amorphous oxide shell. The broken and dangling Al bond could form new Al-O pairs with neighbor oxygen atoms. This bond switching mechanism could promote the viscous flow of the amorphous oxide shell. Meanwhile, the migration of atom clusters during the viscous flow can heal damage in the amorphous native oxide shell before the nucleation of large cavities [15], thus leading to high elongation of the native oxide shell. With the strong confinement of the oxide shell, the internal Al-4Cu single crystal could deform homogeneously without easy slip localization, and thus the nanoscale Al-4Cu alloy tested at a low strain rate with e-beam irradiation could display marked ductility. It should be noted that the Al-4Cu samples with the amorphous oxide shell strained at 5×10^{-3} s^{-1} under e-beam irradiation show brittle fracture, which means that e-beam irradiation-induced viscous flow occurs only at lower strain rates, and this phenomenon is called the velocity-

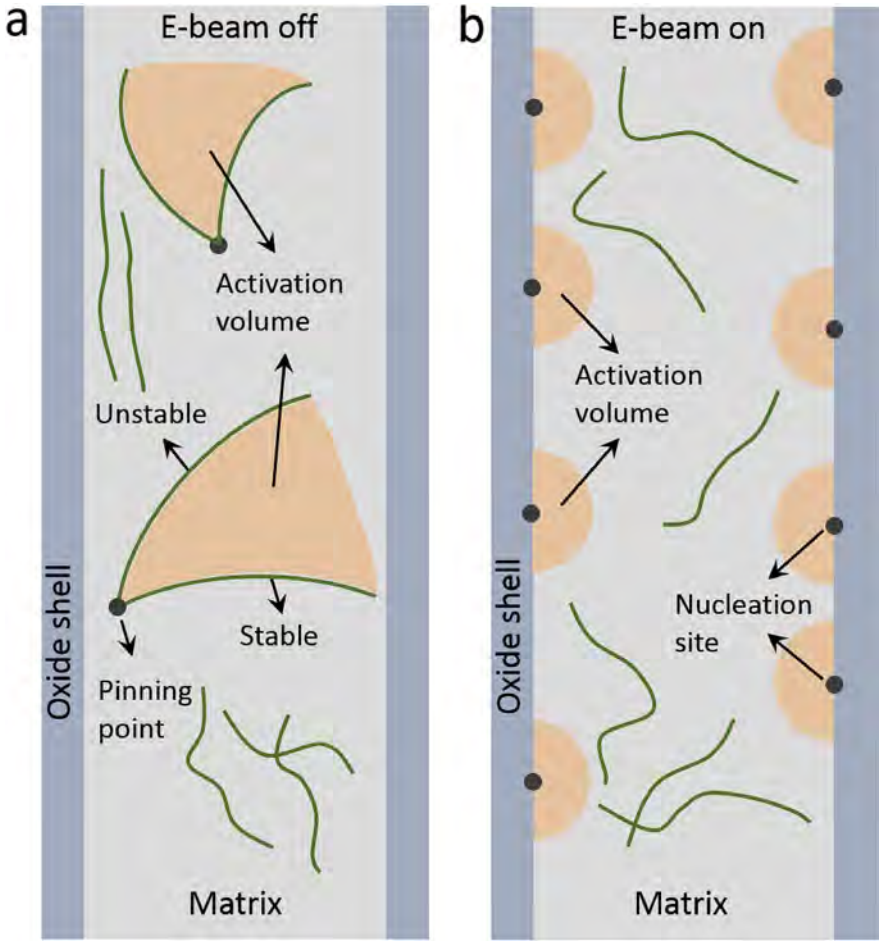

Fig. 9. Schematics illustration of different dislocation nucleation mechanisms in nanoscale Al-4Cu samples under beam on/off conditions at strain rate below 5×10^{-3} s^{-1}. E-beam induces a transition from single-arm source dislocation nucleation **(a)** to interface mediated dislocation nucleation **(b)**.

limited viscous flow of the oxide shell under e-beam irradiation [23]. Under high strain rates, the oxide shell is difficult to deform via viscous flow, and it will be cut through by the accumulated dislocations, resulting in the brittle fracture of whole tensile samples [22]. This behavior explains the observed similar deformation behaviors of small-volume Al-4Cu alloy deformed at high strain rates (5×10^{-2} s^{-1} and 5×10^{-3} s^{-1}) under beam-on and beam-off conditions (Fig. 2). Our tests show that the critical strain rate for deformation of the amorphous oxide shell through viscous flow should be approximately 5×10^{-3} s^{-1}, but the exact value for this transition needs further study. The above analyses are also supported by the PTP tests shown in Fig. 7, in which a higher volume fraction of native oxide shell will enhance the fraction of viscous flow during tensile deformation under e-beam irradiation. The Al with a 29% volume fraction of surface oxide shell delivers ultrahigh uniform elongation, which can be attributed to the combined effects of the e-beam irradiation-induced viscous flow of the amorphous native oxide shell and the Al oxide shell-confined homogeneous plastic deformation of the Al single crystal. This elongation is direct experimental evidence that the e-beam irradiation significantly influences the plasticity of the nanoscale Al sample via influencing the viscous flow of the surface native oxide shell.

5. Conclusion

We systematically investigated the effect of a high-energy (200 keV) e-beam on the deformation behavior of small-volume Al-4Cu alloy. While it is often assumed that high-energy e-beams have negligible influence on the intrinsic mechanical behavior of nanoscale metals, we found here that e-beam irradiation could influence the deformability and strain rate sensitivity of small-volume Al alloy by tuning the viscous flow of the ultrathin amorphous native oxide shell on the surface. A transition from single-arm source (collective dislocation behavior) to interface dislocation nucleation was observed in nanoscale Al-4Cu alloy with the aid of e-beam irradiation. In addition, we found that the combined effects of the e-beam-enhanced viscous flow of the amorphous native oxide shell and the strong confinement of the oxide shell on an Al resulted in high deformability in small-volume Al alloy pulled below a critical strain rate.

Acknowledgements

This work was supported by the National Natural Science Foundation of China (Grant Nos.51471128, 51621063). W.Z.H. would like to thank the support of the National Key Research and Development Program of China (2017YFB0702301), the Youth Thousand Talents Program of China and the Young Talent Support Plan of XJTU. We appreciate the critical reading by Prof. Evan Ma and Prof. Ju Li.

References

[1] M.D. Uchic, D.M. Dimiduk, J.N. Florando, W.D. Nix, Sample dimensions influence strength and crystal plasticity, Science 305 (2004) 986–990.
[2] J.R. Greer, W.C. Oliver, W.D. Nix, Size dependence of mechanical properties of gold at the micro scale in the absence of strain gradients, Acta Mater. 53 (2005) 1821–1830.
[3] J.R. Greer, J.T.M. De Hosson, Plasticity in small-sized metallic systems: intrinsic versus extrinsic size effect, Prog. Mater. Sci. 56 (2011) 654–724.
[4] K.S. Ng, A.H.W. Ngan, Stochastic nature of plasticity of aluminum micro-pillars, Acta Mater. 56 (2008) 4762–4770.
[5] Z.W. Shan, R.K. Mishra, S.A.S. Asif, O.L. Warren, A.M. Minor, Mechanical annealing and source-limited deformation on submicrometer-diameter Ni crystals, Nat. Mater. 7 (2008) 115–119.
[6] S.H. Oh, M. Legros, D. Kiener, G. Dehm, In situ observation of dislocation nucleation and escape in a submicrometer aluminum single crystal, Nat. Mater. 8 (2009) 95–100.
[7] L. Huang, Q.J. Li, Z.W. Shan, J. Li, J. Sun, E. Ma, A new regime for mechanical annealing and strong sample-size strengthening in body centred cubic molybdenum, Nat. Commun. 2 (2011) 547.
[8] Z.J. Wang, Q.J. Li, Z.W. Shan, J. Li, J. Sun, E. Ma, Sample size effects on the large strain bursts in submicro aluminum pillars, Appl. Phys. Lett. 100 (2012) 0719906.
[9] M.S. Ding, J.P. Du, L. Wan, S. Ogata, L. Tian, E. Ma, W.Z. Han, J. Li, Z.W. Shan, Radiation-induced helium nanobubbles enhance ductility in submicro-sized single-crystalline copper, Nano Lett. 16 (2016) 4118–4124.
[10] R.F. Egerton, P. Li, M. Malac, Radiation damage in the TEM and SEM, Micron 35 (2004) 399–409.
[11] R.F. Egerton, R. McLeod, F. Wang, M. Malac, Basic questions related to electron-induced sputtering in the TEM, Ultramicroscopy 110 (2010) 991–997.
[12] R.F. Egerton, Control of radiation damage in the TEM, Ultramicroscopy 127 (2013) 100–108.
[13] F.K. Komissarenko, I.S. Mukhin, A.o. Golubox, N.V. Nikonorov, M.A. Prosnikov, A.I. Sidorov, Effect of electron beam irradiation on the thin metal films on glass surfaces in a submicrometer scale, J. Nanolithogr. Mems Moems 15 (2016) 013502.
[14] P.M. Ajayan, S. Lijima, Electron-beam-enhanced flow and instability in amorphous silica fibers and tips, Phil. Mag. Lett. 65 (1992) 43–48.
[15] K. Zheng, C.C. Wang, Y.Q. Cheng, Y.H. Yue, X.D. Han, Z. Zhang, Z.W. Shan, S.X. Mao, M.M. Ye, Y.D. Yin, E. Ma, Electron-beam-assisted superplastic shaping of nanoscale amorphous silica, Nat. Commun. 1 (2010) 24.
[16] H. Zheng, Y. Liu, S.X. Mao, J.B. Wang, J.Y. Huang, Beam-assisted large elongation of in situ formed Li2O nanowires, Sci. Rep. 2 (2012) 542.
[17] J.F. Zhang, L.H. Bao, R.A. Webb, X.D. Li, Electron beam irradiation stiffens zinc tin oxide nanowires, Nano Lett. 11 (2011) 4885–4889.
[18] Y.H. Yue, K. Zheng, Strong strain rate effect on the plasticity of amorphous silica nanowires, Appl. Phy. Lett. 104 (2014) 231906.
[19] J.H. Luo, J.W. Wang, E. Bitzek, J.Y. Huang, H. Zheng, L.M. Tong, Q. Yang, J. Li, S.X. Mao, Size-dependent brittle-to-ductile transition in silica glass nanofiber, Nano Lett. 16 (2016) 105–113.
[20] R. Sarkar, C. Rentenberger, J. Rajagopalan, Electron beam induced artifacts during in situ TEM deformation of nanostructured metals, Sci. Rep. 5 (2015) 16345.
[21] A.F. Sprecher, S.L. Mannan, H. Conrad, Overview no. 49: on the mechanisms for the electroplastic effect in metals, Acta Metall. 34 (1986) 1145–1162.
[22] S.H. Li, W.Z. Han, J. Li, E. Ma, Z.W. Shan, Small-volume aluminum alloys with native oxide shell deliver unprecedented strength and toughness, Acta Mater. 126 (2017) 202–209.
[23] F.G. Sen, A.T. Alpas, A.C.T. Duin, Y. Qi, Oxidation-assisted ductility of aluminum nanowires, Nat. Commun. 5 (2014) 3959.
[24] F.G. Sen, Y. Qi, A.C.T. Duin, A.T. Alpas, Oxidation induced softening in Al nanowires, Appl. Phys. Lett. 102 (2013) 051912.
[25] A. Bianconi, Al-Al_2O_3 interface study using surface soft-x-ray absorption and photoemission spectroscopy, Phys. Rev. B 19 (1979) 2837–2843.
[26] D.G. Xie, Z.J. Wang, J. Sun, J. Li, E. Ma, Z.W. Shan, *In situ* study of the initiation of hydrogen bubbles at the aluminum metal/oxide interface, Nat. Mater. 14 (2015) 899–904.
[27] M. Li, D.G. Xie, E. Ma, J. Li, X.X. Zhang, Z.W. Shan, Effect of hydrogen on the integrity of aluminum-oxide interface at elevated temperatures, Nat. Commun. 8 (2017) 14564.
[28] F. Mompiou, M. Legros, A. Sedlmayr, D.S. Gianola, D. Caillard, O. Kraft, Source-based strengthening of sub-micrometer Al fibers, Acta Mater. 60 (2012) 977–983.
[29] W.Z. Han, L. Huang, S. Ogata, H. Kimizuka, Z.C. Yang, C. Weiberger, Q.J. Li, B.Y. Liu, X.X. Zhang, J. Li, E. Ma, Z.W. Shan, From “smaller is stronger” to “size-independent strength plateau”: towards measuring the ideal strength of iron, Adv. Mater. 27 (2015) 3385–3390.
[30] W.Z. Han, A. Vinogradov, C.R. Hutchinson, On the reversibility of dislocation slip during cyclic deformation of Al alloys containing shear-resistant particles, Acta Mater. 59 (2011) 3720–3736.
[31] J.D. Teixeira, D.G. Cram, L. Bourgeois, T.J. Bastow, A.J. Hill, C.R. Hutchinson, On the strengthening response of aluminum alloys containing shear-resistant plate-shaped precipitates, Acta Mater. 56 (2008) 6109–6122.
[32] M.S. Ding, L. Tian, W.Z. Han, J. Li, E. Ma, Z.W. Shan, Nanobubble fragmentation and bubble-free-channel shear localization in helium-irradiated submicron-sized copper, Phys. Rev. Lett. 117 (2016) 215501.
[33] J. May, H.W. Hoppel, M. Goken, Strain rate sensitivity of ultrafine-grained aluminum processed by severe plastic deformation, Scr. Mater. 53 (2005) 189–194.
[34] D.S. Gianola, D.H. Warner, J.F. Molinari, K.J. Hemker, Increased strain rate sensitivity due to stress-coupled grain growth in nanocrystalline Al, Scr. Mater. 55 (2006) 649–652.
[35] J.M. Wheeler, V. Maier, K. Durst, M. Goken, J. Michler, Activation parameters for deformation of ultrafine-grained aluminum as determined by indentation strain rate jumps at elevated temperature, Mater. Sci. Eng. A 585 (2013) 108–113.
[36] E. Izadi, J. Rajagopalan, Texture dependent strain rate sensitivity of ultrafine-grained aluminum films, Scr. Mater. 114 (2016) 65–69.
[37] P. Cavaliere, Strain rate sensitivity of ultra-fine and nanocrystalline metals and alloys, Phys. B 403 (2008) 569–575.
[38] J. Chen, L. Lu, K. Lu, Hardness and strain rate sensitivity of nanocrystalline Cu, Scr. Mater. 54 (2006) 1913–1918.
[39] Q. Wei, S. Cheng, K.T. Ramesh, E. Ma, Effect of nanocrystalline and ultrafine grain sizes on the strain rate sensitivity and activation volume: fcc versus bcc metals, Mater. Sci. Eng. A 381 (2004) 71–79.
[40] R. Huang, Q.J. Li, Z.J. Wang, L. Huang, J. Li, E. Ma, Z.W. Shan, Flow stress in submicron BCC iron single crystals: sample-size-dependent strain-rate sensitivity and rate-dependent size strengthening, Mater. Res. Lett. 3 (2015) 121–127.
[41] A.T. Jennings, J. Li, J.R. Greer, Emergence of strain-rate sensitivity in Cu nanopillars: transition from dislocation multiplication to dislocation nucleation, Acta Mater. 59 (2011) 5627–5637.
[42] R.J. Asaro, S. Suresh, Mechanistic models for the activation volume and rate sensitivity in metals with nanocrystalline grains and nano-scale twins, Acta Mater. 53 (2005) 3369–3382.
[43] L. Lu, R. Schwaiger, Z.W. Shan, M. Dao, K. Lu, S. Suresh, Nano-sized twins induce high rate sensitivity of flow stress in pure copper, Acta Mater. 53 (2005) 2169–2179.
[44] M. Dao, L. Lu, Y.F. Shen, S. Suresh, Strength, strain-rate sensitivity and ductility of copper with nanoscale twins, Acta Mater. 54 (2006) 5421–5432.
[45] J.Y. Zhang, G. Liu, J. Sun, Strain rate effects on the mechanical response in the multi-and single-crystalline Cu micropillars: grain boundary effects, Inter. J. Plast. 50 (2013) 1–17.
[46] A. Paul, U. Ramamurty, Strain rate sensitivity of a closed-cell aluminum foam, Mater. Sci. Eng. A 281 (2000) 1–7.
[47] Y.M. Wang, A.V. Hamza, E. Ma, Temperature-dependent strain rate sensitivity and activation volume of nanocrystalline Ni, Acta Mater. 54 (2006) 2715–2726.
[48] J. Sun, L.B. He, Y.-C. Lo, T. Xu, H.C. Bi, L.T. Sun, Z. Zhang, S.X. Mao, J. Li, Liquid-like pseudoelasticity of sub-10-nm crystalline silver particles, Nat. Mater. 13 (2014) 1007–1012.
[49] J.H. Luo, F.F. Wu, J.Y. Huang, J.Q. Wang, S.X. Mao, Superelongation and atomic chain formation in nanosized metallic glass, Phys. Rev. Lett. 104 (2010) 215503.
[50] S.Y. Xu, M.L. Tian, J.G. Wang, J. Xu, J.M. Redwing, M.H.W. Chan, Nanometer-scale modification and welding of silicon and metallic nanowires with a high-intensity electron beam, Small 1 (2005) 1221–1229.
[51] The ESTAR program: stopping-power and range tables for electrons. http://physics.nist.gov/PhysRefData/Star/Text/ESTAR.html.
[52] H.K. Lyeo, D.G. Cahill, Thermal conductance of interfaces between highly dissimilar materials, Phys. Rev. B 73 (2006) 144301.
[53] L.S. Fletcher, Recent development in contact conductance heat transfer, J. Heat. Transf. 110 (1988) 1059–1070.
[54] T. Zhu, J. Li, A. Samanta, A. Leach, K. Gall, Temperature and strain-rate dependence of surface dislocation nucleation, Phys. Rev. Lett. 100 (2008) 025502.
[55] S.H. Oh, M. Legros, D. Kiener, G. Dehm, In situ observation of dislocation nucleation and escape in a submicrometre aluminum single crystal, Nat. Mater. 8 (2009) 95–100.
[56] Y. Lu, J.Y. Huang, C. Wang, S.H. Sun, J. Lou, Cold welding of ultrathin gold nanowires, Nat. Nanotech. 5 (2010) 218–224.
[57] H. Zheng, A.J. Cao, C.R. Weinberger, J.Y. Huang, K. Du, J.B. Wang, Y.Y. Ma, Y.N. Xia, S.X. Mao, Discrete plasticity in sub-10-nm-sized gold crystals, Nat. Commun. 1 (2010) 144.
[58] P. Gu, M. Dao, R.J. Asaro, S. Suresh, A unified mechanistic model for size-dependent deformation in nanocrystalline and nanotwinned metals, Acta Mater. 59 (2011) 6861–6868.